

Evaluating Computational Pathology Foundation Models for Prostate Cancer Grading under Distribution Shifts

Fredrik K. Gustafsson¹

Mattias Rantalainen^{1,2}

¹Department of Medical Epidemiology and Biostatistics, Karolinska Institutet, Stockholm, Sweden

²MedTechLabs, BioClinicum, Karolinska University Hospital, Solna, Sweden

fredrik.gustafsson@ki.se, mattias.rantalainen@ki.se

Abstract

Foundation models have recently become a popular research direction within computational pathology. They are intended to be general-purpose feature extractors, promising to achieve good performance on a range of downstream tasks. Real-world pathology image data does however exhibit considerable variability. Foundation models should be robust to these variations and other distribution shifts which might be encountered in practice. We evaluate two computational pathology foundation models: UNI (trained on more than 100 000 whole-slide images) and CONCH (trained on more than 1.1 million image-caption pairs), by utilizing them as feature extractors within prostate cancer grading models. We find that while UNI and CONCH perform well relative to baselines, the absolute performance can still be far from satisfactory in certain settings. The fact that foundation models have been trained on large and varied datasets does not guarantee that downstream models always will be robust to common distribution shifts.

Computational pathology utilizes machine learning and computer vision methods to automatically extract useful information from histopathology whole-slide images (WSIs) [2, 7, 10, 13, 40]. Commonly studied applications include histological grading [6, 41, 44], risk stratification [21, 24, 42] and biomarker prediction [3, 11, 33]. Foundation models, i.e. large deep learning models trained on large amounts of data using self-supervised learning [4, 5, 30], have recently become a very popular research direction within computational pathology [1, 9, 16, 29, 31, 43, 46, 49]. Foundation models are intended to be general-purpose feature extractors, promising to achieve good performance on a wide range of downstream tasks. Real-world pathology image data does however exhibit considerable

variability, due to differences in staining and scanning procedures employed at different labs and hospitals [23]. A truly general-purpose foundation model should be robust to these variations and other *distribution shifts* [17, 37] which might be encountered during practical deployment. While previous work in the general machine learning literature has shown that deep learning models can be highly sensitive to distribution shifts [18, 20, 25, 35], this has yet to be studied specifically for computational pathology foundation models. In particular, it is currently unclear whether the large and varied datasets utilized in the training of these models make them robust to commonly encountered distribution shifts, or if the model performance still can break down in certain practical settings. In this work we therefore study these open questions, evaluating foundation model robustness in terms of two common types of distribution shifts.

For this evaluation, we utilize histological grading of prostate cancer biopsy WSIs [6, 41] as our specific practical application. Histological grading is used to provide important prognostic information for patients, categorizing biopsies into five different International Society of Urological Pathology (ISUP) grade groups [14, 15]. With non-tumor biopsies denoted as grade 0, each biopsy WSI is thus assigned an ISUP grade 0–5. We evaluate two different computational pathology foundation models: **UNI** [9] (trained on more than 100 000 WSIs using self-supervised learning) and **CONCH** [29] (trained on more than 1.1 million image-caption pairs using a vision-language objective). While various other recently published foundation models also could be evaluated, UNI and CONCH have been among the best performing models in recent benchmarks [8, 32, 45], and we thus choose to focus on them in this work. We also include **Resnet-IN** (trained on a dataset of natural images) as a baseline, to study the effect of pathology-specific models. Following recent benchmarking studies [8, 32, 45], we evaluate the foundation models by utilizing them as *frozen* patch-level feature extractors in weakly supervised WSI-level prediction models. Specifically, we utilize the

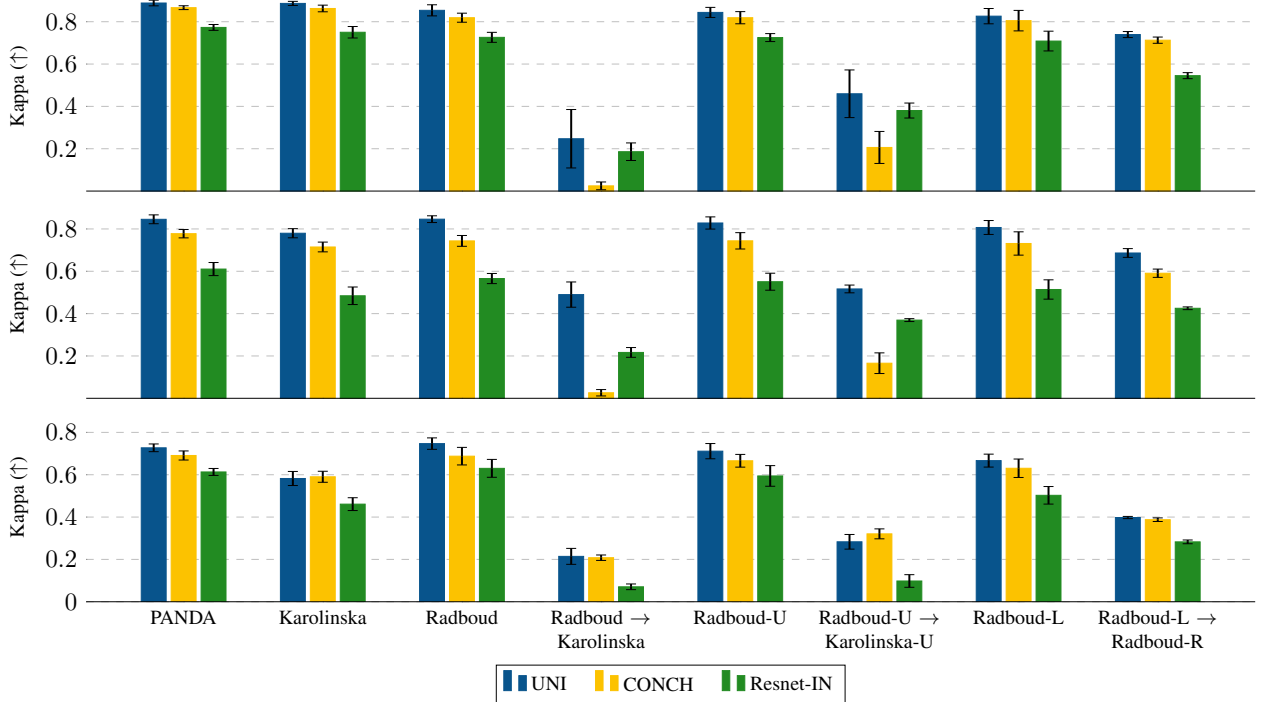


Figure 1. Performance comparison of UNI, CONCH and Resnet-IN across different PANDA subsets, when utilized as patch-level feature extractors in the *ABMIL* (top), *Mean Feature* (middle) or *kNN* (bottom) ISUP grade classification models. All results are mean \pm std (standard deviation) over 10 random cross-validation folds. Raw numerical results for this figure are provided in Table S1 in the supplementary material. The same model performance comparison but in terms of MAE instead of kappa is also found in Figure S1.

foundation model feature extractors in three different ISUP grade classification models (see the *Methods* section for details): *ABMIL* uses attention-based multiple instance learning (ABMIL) [22, 26] to process the patch-level feature vectors and output a predicted ISUP grade $\hat{y}(x) \in \{0, \dots, 5\}$ for each biopsy WSI x . *Mean Feature* removes the trainable ABMIL aggregator and directly feeds the mean patch-level feature vector as input to a small classification network. Lastly, *kNN* removes also this trainable classification network, instead utilizing the k-nearest neighbors algorithm. *kNN* therefore contains no trainable model components, enabling a direct evaluation of the underlying foundation models. We conduct experiments on the PANDA dataset [6], containing 10 616 prostate biopsy WSIs with corresponding ISUP grade labels. The data was collected from two different sites: Radboud University Medical Center (Radboud) in the Netherlands, and Karolinska Institutet (Karolinska) in Sweden. The two sites differ in terms of both the pathology lab procedures and utilized scanners, creating a clear distribution shift for the WSI image data (see Figure 4a). By training ISUP grade models exclusively on Radboud data and then evaluating on Karolinska data, we are thus able to study how robust the foundation models are to this commonly encountered type of distribution

shift. By creating further subsets of the PANDA dataset (see *Methods* for details), we are also able to evaluate foundation model robustness in terms of a second type of distribution shift: shifts in the label distribution over the ISUP grades (see Figure 4b & 4c).

The performance of UNI, CONCH and Resnet-IN across different PANDA subsets is compared in Figure 1, when utilized as patch-level feature extractors in the three ISUP grade models. First, we observe that when models are trained and evaluated on the full PANDA dataset (first column of Figure 1), both UNI and CONCH perform well (0.888 ± 0.013 kappa for UNI with *ABMIL*) and outperform Resnet-IN. Similar results are achieved also when ISUP grade models are both trained and evaluated exclusively on data from either Karolinska or Radboud (second and third column of Figure 1, respectively). However, when models are trained on Radboud data and evaluated on Karolinska data (*Radboud* \rightarrow *Karolinska* in Figure 1), the performance drops drastically (0.247 ± 0.138 kappa for UNI with *ABMIL*). This clear performance drop is observed for all three ISUP grade models, i.e. even when applying kNN directly on top of the foundation model patch-level features. When repeating this experiment on subsets with perfectly uniform ISUP grade label distributions (*Radboud-U* and *Radboud-U*

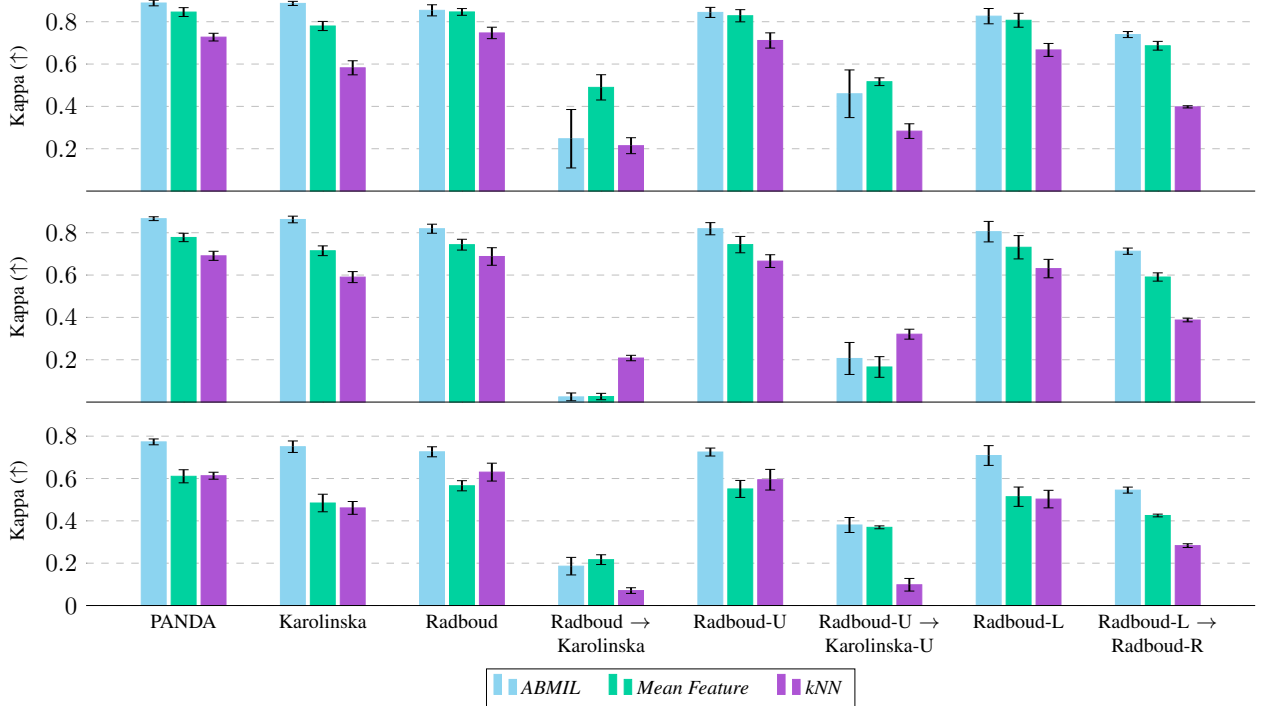


Figure 2. Performance comparison of the ISUP grade models *ABMIL*, *Mean Feature* and *kNN*, when utilizing UNI (**top**), CONCH (**middle**) or Resnet-IN (**bottom**) as patch-level feature extractors. This figure contains the same results as Figure 1, but presented to enable a direct comparison of the ISUP grade models. All results are mean \pm std over 10 random cross-validation folds. Raw numerical results for this figure are provided in Table S2. The same model performance comparison but in terms of MAE instead of kappa is also found in Figure S2.

\rightarrow *Karolinska-U* in Figure 1), the performance drop from Radboud to Karolinska data is somewhat smaller but still highly significant. When models instead are trained and evaluated on Radboud data with left- or right-skewed label distributions (*Radboud-L* and *Radboud-L* \rightarrow *Radboud-R* in Figure 1), there is a consistent but relatively small drop in performance, at least for the *ABMIL* and *Mean Feature* ISUP grade models. Figure 2 contains the same results as Figure 1, but presented in order to enable a direct performance comparison of the three ISUP grade models. We observe that *ABMIL* achieves the best performance in most cases across the different PANDA subsets and feature extractors, followed by *Mean Feature* and *kNN*. The ranking of the three models is more varied for *Radboud* \rightarrow *Karolinska* and *Radboud-U* \rightarrow *Karolinska-U*, but for these cases relatively poor performance is achieved by all three models.

A more detailed performance comparison of UNI, CONCH and Resnet-IN is given in Figure 3 (top), when utilized in the *ABMIL* ISUP grade model. The left and middle plots show how the performance on Radboud and Karolinska test data, respectively, is affected when training models on varying amounts of Radboud data. While the performance on Radboud (in-distribution, ID) data consistently improves with more training data, this is not the case on

Karolinska (out-of-distribution, OOD) data. We also observe that UNI and CONCH perform especially well relative to Resnet-IN when the amount of training data is limited. The right plot of Figure 3 (top) shows how the performance on Karolinska test data is affected when varying the proportion of training data sampled from Karolinska. There, we observe that when increasing from 0% Karolinska training data, the performance quickly improves to a level close to that achieved with 100% Karolinska training data. We also observe in Figure 3 (top) that in most cases, UNI achieves the best performance closely followed by CONCH, with a bigger drop down to Resnet-IN. Figure 3 (bottom) shows the same performance comparison but for the three ISUP grade models instead, when using UNI as the patch-level feature extractor. We observe that, in virtually all cases, *ABMIL* achieves the best performance followed by *Mean Feature* and *kNN*.

UNI outperforms Resnet-IN in every single setting across Figure 1 & 3. Relative to this baseline which is trained on natural images, the pathology-specific foundation model UNI thus achieves very strong performance, as expected. However, the absolute performance of UNI is still poor for *Radboud* \rightarrow *Karolinska* and *Radboud-U* \rightarrow *Karolinska-U* in Figure 1. That is, ISUP grade mod-

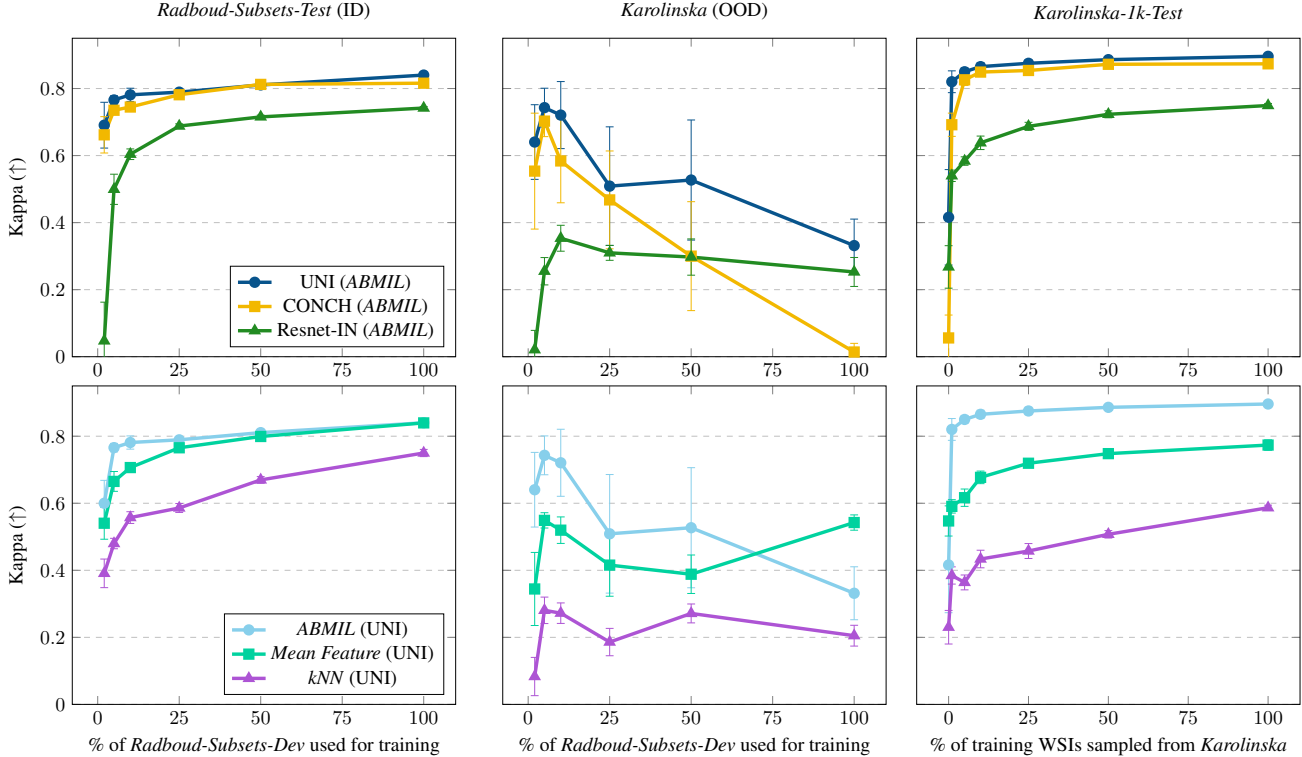
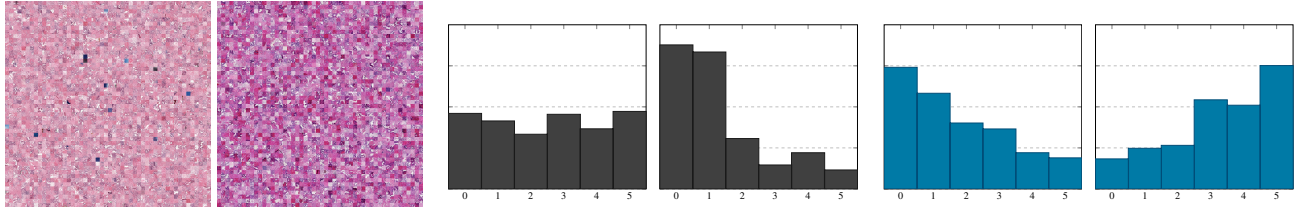


Figure 3. **Top:** Detailed performance comparison of UNI, CONCH and Resnet-IN, when utilized as patch-level feature extractors in the *ABMIL* ISUP grade model. **Bottom:** Detailed performance comparison of the three ISUP grade models *ABMIL*, *Mean Feature* and *kNN*, when utilizing UNI as the patch-level feature extractor. All results are mean \pm std over 10 random cross-validation folds.

els based on UNI are still highly sensitive to the distribution shift from Radboud to Karolinska data. Models based on CONCH seem to be even more sensitive to this distribution shift, given that CONCH even is outperformed by Resnet-IN in most settings for *Radboud* \rightarrow *Karolinska* and *Radboud-U* \rightarrow *Karolinska-U* in Figure 1. The fact that UNI and CONCH have been trained on very large and varied datasets (UNI: more than 100 000 WSIs, CONCH: more than 1.1 million image-caption pairs) does therefore *not* guarantee that models built on top of UNI or CONCH always will perform well in downstream prediction tasks. The quality of the data used to fit the actual downstream models is still crucially important. If this data has limited variability in terms of the number of data collection sites or utilized scanners, downstream models can still become highly sensitive to commonly encountered distribution shifts. While pathology-specific foundation models achieve very strong performance *relative* to general baselines such as Resnet-IN, the *absolute* performance can still be far from satisfactory in certain settings. When comparing the two foundation models UNI and CONCH in Figure 1 & 3, UNI achieves at least slightly better performance in almost all cases. This is somewhat surprising, given that the vision-language model CONCH was found superior in the recent

benchmarking study by Neidlinger & El Nahhas et al. [32]. Moreover, the results for *Radboud-U* \rightarrow *Karolinska-U* and *Radboud-L* \rightarrow *Radboud-R* in Figure 1 strongly suggest that shifts in the label distribution over ISUP grades are small issues compared to the WSI image data shift. The results in the middle plots of Figure 3 might initially seem quite surprising (training on more data tends to degrade the model OOD generalizability). However, if models are trained on large amounts of data from just a single site, it seems reasonable that this effectively could cause models to overfit to that one particular site. Lastly, the comparison of ISUP grade models in Figure 2 & 3 demonstrates added benefit overall of utilizing a trainable ABMIL aggregator and classification layer.

The main actionable takeaways from our study can be summarized as follows: 1. While the computational pathology foundation models UNI and CONCH achieve very strong performance *relative* to the Resnet-IN baseline, the *absolute* performance can still be far from satisfactory in certain settings. 2. The fact that UNI and CONCH have been trained on very large and varied datasets does *not* guarantee that downstream prediction models always will be robust to commonly encountered distribution shifts. 3. Even within the emerging paradigm of powerful



(a) WSI image data shift, *Radboud* \rightarrow *Karolinska*. (b) Grade label shift, *Radboud* \rightarrow *Karolinska*. (c) Grade label shift, *Radboud-L* \rightarrow *Radboud-R*.

Figure 4. We study robustness in terms of two common types of distribution shifts: (a): Shifts in the WSI image data (visualization of 2 500 randomly sampled patches from *Radboud* and *Karolinska*). (b) & (c): Shifts in the label distribution over the ISUP grades 0 – 5.

pathology-specific foundation models, the quality of the data utilized to fit downstream prediction models is a crucial aspect. 4. The vision-only model UNI outperforms the vision-language model CONCH overall. 5. Models are less sensitive to grade label distribution shifts than to WSI image data shifts.

The results in the right plots of Figure 3 suggest that it might be sufficient to add relatively small amounts of training data from a second site to improve the model generalizability. The current experiment does however not provide conclusive evidence for this claim, since both the training and test sets here contain data from the same site. It would therefore be interesting to instead conduct experiments with data from three different sites in future work (for example, study if a model trained on 50% site 1 data and 50% site 2 data generalizes better to site 3, than a model trained on 100% site 1 data). More generally, it would be interesting to study how well models trained on data from $n = 1, 2, 3, \dots$ different sites perform on site $n + 1$. The robustness of other recent foundation models [39, 43, 46, 49] could also be evaluated. If clear differences among the different models were to be discovered, this would be important information to consider when employing foundation models in various practical applications.

Methods

Experimental Setup

We conduct all experiments using the publicly available development set of the PANDA dataset [6]. It contains 10 616 prostate biopsy WSIs with corresponding ISUP grade labels (grade 0 – 5). The 10 616 biopsy WSIs were collected from two different sites: Radboud University Medical Center (Nijmegen, the Netherlands) and Karolinska Institutet (Stockholm, Sweden). The 10 616 WSIs were collected from a total of 2 113 patients. The data collection site (Radboud or Karolinska) is known for each WSI in the dataset, while there is no available information on which patient each WSI originates from.

The WSIs from the two data collection sites were digitally scanned using different scanners (Radboud: 3DHIS-

tech, Karolinska: Leica or Hamamatsu). Together with other potential differences in staining and processing procedures, this creates a clear shift in appearance of the corresponding WSI image data, as shown in Figure 4a (visualization of randomly sampled tissue patches from Radboud and Karolinska WSIs).

Following the PANDA challenge [6], model performance is evaluated using quadratically weighted Cohen’s kappa (‘kappa’ for short) as the main metric, which measures the level of agreement between the predicted and ground truth ISUP grades. As a secondary metric, we also compute the mean absolute error (MAE) between grade predictions and labels.

Main Evaluation For the main model comparison in Figure 1 & 2, we create different subsets of the original PANDA development set, resulting in 7 different datasets in total. **1. PANDA** is the full original dataset, containing 10 433 WSIs after pre-processing (removal of WSIs with no extracted tissue patches). **2. Karolinska** is a subset of PANDA, containing all WSIs collected at Karolinska, 5 434 WSIs. Similarly, **3. Radboud** contains all WSIs collected at Radboud, 4 999 WSIs. The label distribution for *Radboud* and *Karolinska*, as shown in Figure 4b, are quite different: nearly a uniform distribution over grade 0 – 5 for *Radboud*, whereas the distribution is heavily left-skewed for *Karolinska*. In order to study the effect of this label shift, we create further subsets with a perfectly uniform label distribution: **4. Radboud-U** containing 3 996 WSIs, and **5. Karolinska-U** containing 1 506 WSIs. We also create subsets of *Radboud* with a left-skewed or right-skewed label distribution (as shown in Figure 4c): **6. Radboud-L** containing 2 484 WSIs, and **7. Radboud-R** containing 2 515 WSIs.

For the PANDA, *Karolinska*, *Radboud*, *Radboud-U* and *Radboud-L* results in Figure 1 & 2, all models are trained and evaluated using random 10-fold cross-validation (80%/10%/10% train/val/test splits). For the *Radboud* \rightarrow *Karolinska*, *Radboud-U* \rightarrow *Karolinska-U* and *Radboud-L* \rightarrow *Radboud-R* results, the 10 trained cross-validation models are all evaluated on the full corresponding test set (e.g. for *Radboud* \rightarrow *Karolinska*, the 10 models trained on *Rad-*

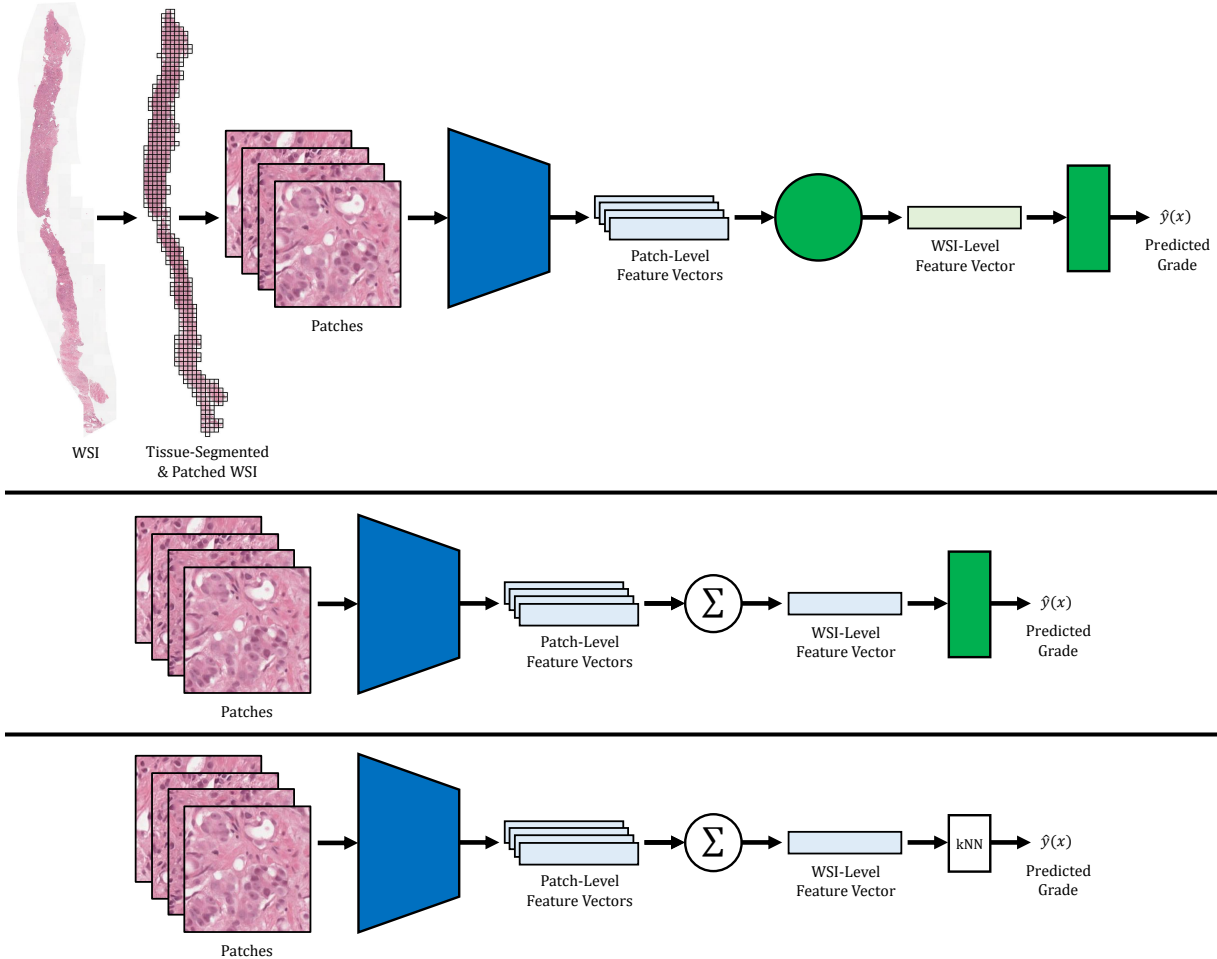


Figure 5. Overview of the three evaluated ISUP grade classification models: **Top: ABMIL**. **Middle: Mean Feature**. **Bottom: kNN**. All three models utilize the same initial WSI processing steps. First, the input prostate biopsy WSI x is tissue-segmented and divided into non-overlapping patches \tilde{x}_i of size 256×256 using CLAM [28]. Next, a feature vector $p(\tilde{x}_i)$ is extracted for each patch, using a pretrained and frozen feature extractor (either UNI [9], CONCH [29] or Resnet-IN). The different models then process these patch-level feature vectors $p(\tilde{x}_i)$ further (see the *Methods* section for details), finally outputting a predicted ISUP grade $\hat{y}(x) \in \{0, \dots, 5\}$. In all three figures, **blue** marks the pretrained and *frozen* patch-level feature extractor, whereas **green** marks trainable model components.

boud are all evaluated on *Karolinska*).

Detailed Evaluation For the detailed model comparison in Figure 3, we create additional subsets of *Radboud* and *Karolinska*. For the left and middle plots of Figure 3, we set aside 1000 randomly sampled WSIs from *Radboud* to form *Radboud-Subsets-Test*, while the remaining 3999 WSIs form *Radboud-Subsets-Dev-100*. We then also create *Radboud-Subsets-Dev-50*, *Radboud-Subsets-Dev-25*, *Radboud-Subsets-Dev-10*, *Radboud-Subsets-Dev-5* and *Radboud-Subsets-Dev-2*, by randomly sampling 50%, 25%, 10%, 5% or 2% of the WSIs in *Radboud-Subsets-Dev-100*. The *Radboud-Subsets-Dev* datasets are used for training models (random 10-fold cross-validation), which then are evaluated on both *Radboud-Subsets-Test* and *Karolinska*.

For the right plots of Figure 3, we set aside 1000 randomly sampled WSIs from *Karolinska* to form *Karolinska-1k-Test*. We then randomly sample the remaining 4434 WSIs from *Karolinska* and all 4999 WSIs of *Radboud*, to form a series of datasets all containing 4000 WSIs, with 0%, 1%, 5%, 10%, 25%, 50% or 100% of the WSIs being sampled from *Karolinska*. These mixed *Radboud/Karolinska* datasets are used for training models (random 10-fold cross-validation), which then are evaluated on *Karolinska-1k-Test*.

ISUP Grade Classification Models

We evaluate three different models, which all take a prostate biopsy WSI x as input and output a predicted ISUP grade

$\hat{y}(x) \in \{0, \dots, 5\}$. An overview of the models is shown in Figure 5. Although there is an ordinal relationship among the 6 ISUP grades $\{0, \dots, 5\}$, we treat this as a regular multi-class classification problem, with $C = 6$ classes.

All three models utilize the same initial WSI processing steps. First, the input biopsy WSI x is tissue-segmented and divided into P non-overlapping patches $\{\tilde{x}_i\}_{i=1}^P$ using CLAM [28]. Patches are of size 256×256 at $20\times$ magnification, and the number of extracted tissue patches P varies for different WSIs. Next, a feature vector $p(\tilde{x}_i)$ is extracted for each patch \tilde{x}_i , using a pretrained and frozen feature extractor. The three models then process these *patch-level* feature vectors $\{p(\tilde{x}_i)\}_{i=1}^P$ further, finally outputting a predicted ISUP grade $\hat{y}(x) \in \{0, \dots, 5\}$ for the WSI x .

ABMIL The first ISUP grade classification model, *ABMIL* in Figure 5 (top), utilizes an ABMIL model [22] to aggregate the set of patch-level feature vectors $\{p(\tilde{x}_i)\}_{i=1}^P$ into a single WSI-level feature vector $w(x)$. This feature vector $w(x)$ is then fed as input to a linear classification layer, outputting logits for the $C = 6$ classes/grades. Finally, $\hat{y}(x) \in \{0, \dots, 5\}$ is computed as the argmax over the logits. Both the ABMIL aggregator and the linear classification layer are trained using the standard cross-entropy loss. Our ABMIL implementation is based on CLAM [28] (without the instance-level clustering), and we set the model and training hyperparameters according to UNI (see *Methods - Weakly supervised slide classification* in [9]). Specifically, models are trained using the AdamW optimizer [27] with a cosine learning rate schedule, for a maximum of 20 epochs. Early stopping is performed based on the val loss for each of the 10 random train/val/test cross-validation folds.

Mean Feature The second model, *Mean Feature* in Figure 5 (middle), simplifies *ABMIL* by removing the trainable ABMIL WSI-level aggregator. Instead, a single WSI-level feature vector $w(x)$ is extracted by directly computing the mean over all patch-level feature vectors $\{p(\tilde{x}_i)\}_{i=1}^P$. The WSI-level feature vector $w(x)$ is then fed as input to a network head consisting of a fully-connected layer (with dropout and ReLU activation) and a linear classification layer, outputting logits for the $C = 6$ classes/grades. The network head (which is the only trainable model component left) is trained using the cross-entropy loss, with the same hyperparameters as used for *ABMIL*.

kNN The third ISUP grade model, *kNN* in Figure 5 (bottom), in turn simplifies *Mean Feature* by removing its trainable network head. As for *Mean Feature*, a WSI-level feature vector $w(x)$ is directly computed as the mean over the patch-level feature vectors $\{p(\tilde{x}_i)\}_{i=1}^P$. To output a predicted ISUP grade $\hat{y}(x) \in \{0, \dots, 5\}$, we then instead utilize `KNeighborsClassifier` from scikit-learn [36]

with $k = 5$. We include *kNN* as a simplest possible baseline, without any trainable model parameters.

Feature Extractors

We utilize three different patch-level feature extractors: UNI, CONCH and Resnet-IN. UNI and Resnet-IN extract patch-level feature vectors $p(\tilde{x}_i)$ of dimension 1 024, whereas CONCH feature vectors are of dimension 512. The feature extractors are kept frozen in all our experiments, i.e. they are not updated during the training of any of the ISUP grade classification models.

UNI [9] is a vision-only foundation model developed specifically for the computational pathology domain. It is a ViT-Large vision transformer [12], pretrained using DINOv2 [34] on a pan-cancer dataset (20 major tissue types) collected from the Massachusetts General Hospital, Brigham & Women’s Hospital and the Genotype-Tissue Expression consortium. This dataset contains roughly 100 million tissue patches from more than 100 000 WSIs.

CONCH [29] is a *vision-language* foundation model, also developed specifically for computational pathology applications. The full CONCH model consists of both an image encoder and a text encoder, but we only utilize the image encoder. This image encoder, which is a ViT-Base vision transformer [12], was first pretrained on an in-house dataset of 16 million tissue patches from more than 21 000 WSIs, using the iBOT [48] self-supervised learning method. Then, the full CONCH model was further pretrained using a vision-language objective, on a dataset containing more than 1.1 million pathology-specific image-caption pairs. This image-caption dataset was curated via automatic processing of figures extracted from publicly available articles from PubMed. The vision-language pretraining objective from CoCa [47] was utilized, which combines image-text contrastive losses and an image captioning loss.

Resnet-IN is a Resnet-50 model [19] pretrained on the ImageNet dataset [38] of natural images. Resnet-IN is included as a simple baseline, expected to be outperformed by the pathology-specific foundation models UNI and CONCH.

Ethics Statement

This study only utilized publicly available and anonymized whole-slide images.

Data Availability

The biopsy whole-slide images and corresponding ISUP grade labels for the development set of the PANDA dataset are available at <https://www.kaggle.com/c/prostate-cancer-grade-assessment/data>.

Code Availability

The code for this study is based on CLAM, UNI and CONCH, which are available at <https://github.com/mahmoodlab/CLAM>, <https://github.com/mahmoodlab/UNI> and <https://github.com/mahmoodlab/CONCH>, respectively. Further implementation details are available from the corresponding author (FKG) upon reasonable request.

Acknowledgments

This work was supported by funding from the Swedish Research Council, the Swedish Cancer Society, VINNOVA (SWAIPP2 project), MedTechLabs, and the Swedish e-science Research Centre (SeRC) - eMPHasis.

Author Contributions

FKG was responsible for project conceptualization, software implementation, preparation of figures and tables, and manuscript drafting. MR was responsible for funding acquisition and project supervision. Both authors contributed to the design of experiments, interpretation of results, and manuscript editing.

Competing Interests

MR is co-founder and shareholder of Stratipath AB. FKG has no competing interests to declare.

References

- [1] Nanne Aben, Edwin D de Jong, Ioannis Gatopoulos, Nicolas Känzig, Mikhail Karasikov, Axel Lagré, Roman Moser, Joost van Doorn, Fei Tang, et al. Towards large-scale training of pathology foundation models. *arXiv preprint arXiv:2404.15217*, 2024. **1**
- [2] Balázs Acs, Mattias Rantalainen, and Johan Hartman. Artificial intelligence as the next step towards precision pathology. *Journal of Internal Medicine*, 288(1):62–81, 2020. **1**
- [3] Salim Arslan, Julian Schmidt, Cher Bass, Debapriya Mehrotra, Andre Geraldes, Shikha Singhal, Julius Hense, Xiusi Li, Pandu Raharja-Liu, Oscar Maiques, et al. A systematic pan-cancer study on deep learning-based prediction of multi-omic biomarkers from routine pathology images. *Communications Medicine*, 4(1):48, 2024. **1**
- [4] Bobby Azad, Reza Azad, Sania Eskandari, Afshin Bozorgpour, Amirhossein Kazerouni, Islem Rekik, and Dorit Merhof. Foundational models in medical imaging: A comprehensive survey and future vision. *arXiv preprint arXiv:2310.18689*, 2023. **1**
- [5] Rishi Bommasani, Drew A Hudson, Ehsan Adeli, Russ Altman, Simran Arora, Sydney von Arx, Michael S Bernstein, Jeannette Bohg, Antoine Bosselut, Emma Brunskill, et al. On the opportunities and risks of foundation models. *arXiv preprint arXiv:2108.07258*, 2021. **1**
- [6] Wouter Bulten, Kimmo Kartasalo, Po-Hsuan Cameron Chen, Peter Ström, Hans Pinckaers, Kunal Nagpal, Yuannan Cai, David F Steiner, Hester Van Boven, Robert Vink, et al. Artificial intelligence for diagnosis and gleason grading of prostate cancer: the PANDA challenge. *Nature Medicine*, 28(1):154–163, 2022. **1, 2, 5**
- [7] Gabriele Campanella, Matthew G Hanna, Luke Geneslaw, Allen Miraflor, Vitor Werneck Krauss Silva, Klaus J Busam, Edi Brogi, Victor E Reuter, David S Klimstra, and Thomas J Fuchs. Clinical-grade computational pathology using weakly supervised deep learning on whole slide images. *Nature Medicine*, 25(8):1301–1309, 2019. **1**
- [8] Gabriele Campanella, Shengjia Chen, Ruchika Verma, Jennifer Zeng, Aryeh Stock, Matt Croken, Brandon Veremis, Abdulkadir Elmas, Kuan-lin Huang, Ricky Kwan, et al. A clinical benchmark of public self-supervised pathology foundation models. *arXiv preprint arXiv:2407.06508*, 2024. **1**
- [9] Richard J Chen, Tong Ding, Ming Y Lu, Drew FK Williamson, Guillaume Jaume, Andrew H Song, Bowen Chen, Andrew Zhang, Daniel Shao, Muhammad Shaban, et al. Towards a general-purpose foundation model for computational pathology. *Nature Medicine*, 30(3):850–862, 2024. **1, 6, 7**
- [10] Didem Cifci, Sebastian Foersch, and Jakob Nikolas Kather. Artificial intelligence to identify genetic alterations in conventional histopathology. *The Journal of Pathology*, 257(4):430–444, 2022. **1**
- [11] Nicolas Coudray, Paolo Santiago Ocampo, Theodore Sakellaropoulos, Navneet Narula, Matija Snuderl, David Fenyö, Andre L Moreira, Narges Razavian, and Aristotelis Tsirigos. Classification and mutation prediction from non-small cell lung cancer histopathology images using deep learning. *Nature Medicine*, 24(10):1559–1567, 2018. **1**
- [12] Alexey Dosovitskiy, Lucas Beyer, Alexander Kolesnikov, Dirk Weissenborn, Xiaohua Zhai, Thomas Unterthiner, Mostafa Dehghani, Matthias Minderer, Georg Heigold, Sylvain Gelly, Jakob Uszkoreit, and Neil Houlsby. An image is worth 16x16 words: Transformers for image recognition at scale. In *International Conference on Learning Representations (ICLR)*, 2021. **7**
- [13] Amelie Echle, Niklas Timon Rindtorff, Titus Josef Brinker, Tom Luedde, Alexander Thomas Pearson, and Jakob Nikolas Kather. Deep learning in cancer pathology: a new generation of clinical biomarkers. *British Journal of Cancer*, 124(4):686–696, 2021. **1**
- [14] Jonathan I Epstein. An update of the gleason grading system. *The Journal of urology*, 183(2):433–440, 2010. **1**
- [15] Jonathan I Epstein, Michael J Zelefsky, Daniel D Sjoberg, Joel B Nelson, Lars Egevad, Cristina Magi-Galluzzi, Andrew J Vickers, Anil V Parwani, Victor E Reuter, Samson W Fine, et al. A contemporary prostate cancer grading system: a validated alternative to the gleason score. *European urology*, 69(3):428–435, 2016. **1**
- [16] Alexandre Filiot, Ridouane Ghermi, Antoine Olivier, Paul Jacob, Lucas Fidon, Alice Mac Kain, Charlie Saillard, and Jean-Baptiste Schiratti. Scaling self-supervised learning for histopathology with masked image modeling. *medRxiv preprint*, 2023. **1**

- [17] Samuel G Finlayson, Adarsh Subbaswamy, Karandeep Singh, John Bowers, Annabel Kupke, Jonathan Zittrain, Isaac S Kohane, and Suchi Saria. The clinician and dataset shift in artificial intelligence. *New England Journal of Medicine*, 385(3):283–286, 2021. [1](#)
- [18] Fredrik K. Gustafsson, Martin Danelljan, and Thomas B. Schön. How reliable is your regression model’s uncertainty under real-world distribution shifts? *Transactions on Machine Learning Research (TMLR)*, 2023. [1](#)
- [19] Kaiming He, Xiangyu Zhang, Shaoqing Ren, and Jian Sun. Deep residual learning for image recognition. In *Proceedings of the IEEE Conference on Computer Vision and Pattern Recognition (CVPR)*, pages 770–778, 2016. [7](#)
- [20] Dan Hendrycks and Thomas Dietterich. Benchmarking neural network robustness to common corruptions and perturbations. In *International Conference on Learning Representations (ICLR)*, 2019. [1](#)
- [21] Julia Höhn, Eva Krieghoff-Henning, Christoph Wies, Lennard Kiehl, Martin J Hetz, Tabea-Clara Bucher, Jitendra Jonnagaddala, Kurt Zatloukal, Heimo Müller, Markus Plass, et al. Colorectal cancer risk stratification on histological slides based on survival curves predicted by deep learning. *npj Precision Oncology*, 7(1):98, 2023. [1](#)
- [22] Maximilian Ilse, Jakub Tomczak, and Max Welling. Attention-based deep multiple instance learning. In *International Conference on Machine Learning (ICML)*, pages 2127–2136, 2018. [2](#), [7](#)
- [23] Mostafa Jahanifar, Manahil Raza, Kesi Xu, Trinh Vuong, Rob Jewsbury, Adam Shephard, Neda Zamanitajeddin, Jin Tae Kwak, Shan E Ahmed Raza, Fayyaz Minhas, et al. Domain generalization in computational pathology: survey and guidelines. *arXiv preprint arXiv:2310.19656*, 2023. [1](#)
- [24] Xiaofeng Jiang, Michael Hoffmeister, Hermann Brenner, Hannah Sophie Muti, Tanwei Yuan, Sebastian Foersch, Nicholas P West, Alexander Brobeil, Jitendra Jonnagaddala, Nicholas Hawkins, et al. End-to-end prognostication in colorectal cancer by deep learning: a retrospective, multicentre study. *The Lancet Digital Health*, 6(1):e33–e43, 2024. [1](#)
- [25] Pang Wei Koh, Shiori Sagawa, Henrik Marklund, Sang Michael Xie, Marvin Zhang, Akshay Balsubramani, Weihua Hu, Michihiro Yasunaga, Richard Lanus Phillips, Irena Gao, et al. Wilds: A benchmark of in-the-wild distribution shifts. In *International Conference on Machine Learning (ICML)*, pages 5637–5664. PMLR, 2021. [1](#)
- [26] Narmin Ghaffari Laleh, Hannah Sophie Muti, Chiara Maria Lavinia Loeffler, Amelie Echle, Oliver Lester Saldanha, Faisal Mahmood, Ming Y Lu, Christian Trautwein, Rupert Langer, Bastian Dislich, et al. Benchmarking weakly-supervised deep learning pipelines for whole slide classification in computational pathology. *Medical Image Analysis*, 79, 2022. [2](#)
- [27] Ilya Loshchilov and Frank Hutter. Decoupled weight decay regularization. In *International Conference on Learning Representations (ICLR)*, 2019. [7](#)
- [28] Ming Y Lu, Drew FK Williamson, Tiffany Y Chen, Richard J Chen, Matteo Barbieri, and Faisal Mahmood. Data-efficient and weakly supervised computational pathology on whole-slide images. *Nature Biomedical Engineering*, 5(6):555–570, 2021. [6](#), [7](#)
- [29] Ming Y Lu, Bowen Chen, Drew FK Williamson, Richard J Chen, Ivy Liang, Tong Ding, Guillaume Jaume, Igor Odintsov, Long Phi Le, Georg Gerber, et al. A visual-language foundation model for computational pathology. *Nature Medicine*, 30:863–874, 2024. [1](#), [6](#), [7](#)
- [30] Michael Moor, Oishi Banerjee, Zahra Shakeri Hossein Abad, Harlan M Krumholz, Jure Leskovec, Eric J Topol, and Pranav Rajpurkar. Foundation models for generalist medical artificial intelligence. *Nature*, 616(7956):259–265, 2023. [1](#)
- [31] Dmitry Nechaev, Alexey Pchelnikov, and Ekaterina Ivanova. Hibou: A family of foundational vision transformers for pathology. *arXiv preprint arXiv:2406.05074*, 2024. [1](#)
- [32] Peter Neidlinger, Omar SM El Nahhas, Hannah Sophie Muti, Tim Lenz, Michael Hoffmeister, Hermann Brenner, Marko van Treeck, Rupert Langer, Bastian Dislich, Hans Michael Behrens, et al. Benchmarking foundation models as feature extractors for weakly-supervised computational pathology. *arXiv preprint arXiv:2408.15823*, 2024. [1](#), [4](#)
- [33] Jan Moritz Niehues, Philip Quirke, Nicholas P West, Heike I Grabsch, Marko van Treeck, Yoni Schirris, Gregory P Veldhuizen, Gordon GA Hutchins, Susan D Richman, Sebastian Foersch, et al. Generalizable biomarker prediction from cancer pathology slides with self-supervised deep learning: A retrospective multi-centric study. *Cell Reports Medicine*, 4(4), 2023. [1](#)
- [34] Maxime Oquab, Timothée Darcet, Théo Moutakanni, Huy V. Vo, Marc Szafraniec, Vasil Khalidov, Pierre Fernandez, Daniel HAZIZA, Francisco Massa, Alaaeldin El-Nouby, Mido Assran, Nicolas Ballas, Wojciech Galuba, Russell Howes, Po-Yao Huang, Shang-Wen Li, Ishan Misra, Michael Rabbat, Vasu Sharma, Gabriel Synnaeve, Hu Xu, Herve Jegou, Julien Mairal, Patrick Labatut, Armand Joulin, and Piotr Bojanowski. DINOv2: Learning robust visual features without supervision. *Transactions on Machine Learning Research (TMLR)*, 2024. [7](#)
- [35] Yaniv Ovadia, Emily Fertig, Jie Ren, Zachary Nado, D. Sculley, Sebastian Nowozin, Joshua Dillon, Balaji Lakshminarayanan, and Jasper Snoek. Can you trust your model’s uncertainty? Evaluating predictive uncertainty under dataset shift. In *Advances in Neural Information Processing Systems (NeurIPS)*, 2019. [1](#)
- [36] F. Pedregosa, G. Varoquaux, A. Gramfort, V. Michel, B. Thirion, O. Grisel, M. Blondel, P. Prettenhofer, R. Weiss, V. Dubourg, J. Vanderplas, A. Passos, D. Cournapeau, M. Brucher, M. Perrot, and E. Duchesnay. Scikit-learn: Machine learning in Python. *Journal of Machine Learning Research (JMLR)*, 12:2825–2830, 2011. [7](#)
- [37] Joaquin Quionero-Candela, Masashi Sugiyama, Anton Schwaighofer, and Neil D Lawrence. Dataset shift in machine learning, 2009. [1](#)
- [38] Olga Russakovsky, Jia Deng, Hao Su, Jonathan Krause, Sanjeev Satheesh, Sean Ma, Zhiheng Huang, Andrej Karpathy, Aditya Khosla, Michael Bernstein, et al. Imagenet large

- scale visual recognition challenge. *International Journal of Computer Vision (IJCV)*, 115:211–252, 2015. 7
- [39] Charlie Saillard, Rodolphe Jenatton, Felipe Llinares-López, Zeldia Mariet, David Cahané, Eric Durand, and Jean-Philippe Vert. H-optimus-0, 2024. 5
- [40] Artem Shmatko, Narmin Ghaffari Laleh, Moritz Gerstung, and Jakob Nikolas Kather. Artificial intelligence in histopathology: enhancing cancer research and clinical oncology. *Nature Cancer*, 3(9):1026–1038, 2022. 1
- [41] Peter Ström, Kimmo Kartasalo, Henrik Olsson, Leslie Solorzano, Brett Delahunt, Daniel M Berney, David G Bostwick, Andrew J Evans, David J Grignon, Peter A Humphrey, et al. Artificial intelligence for diagnosis and grading of prostate cancer in biopsies: a population-based, diagnostic study. *The Lancet Oncology*, 21(2):222–232, 2020. 1
- [42] Sarah Volinsky-Fremont, Nanda Horeweg, Sonali Andani, Jurriaan Barkey Wolf, Maxime W Lafarge, Cor D de Kroon, Gitte Ørtoft, Estrid Høgdall, Jouke Dijkstra, Jan J Jobsen, et al. Prediction of recurrence risk in endometrial cancer with multimodal deep learning. *Nature Medicine*, pages 1–12, 2024. 1
- [43] Eugene Vorontsov, Alican Bozkurt, Adam Casson, George Shaikovski, Michal Zelechowski, Kristen Severson, Eric Zimmermann, James Hall, Neil Tenenholtz, Nicolo Fusi, et al. A foundation model for clinical-grade computational pathology and rare cancers detection. *Nature Medicine*, pages 1–12, 2024. 1, 5
- [44] Y Wang, B Acs, S Robertson, B Liu, Leslie Solorzano, Carolina Wählby, J Hartman, and M Rantalainen. Improved breast cancer histological grading using deep learning. *Annals of Oncology*, 33(1):89–98, 2022. 1
- [45] Georg Wölflein, Dyke Ferber, Asier R. Meneghetti, Omar S. M. El Nahhas, Daniel Truhn, Zunamys I. Carrero, David J. Harrison, Ognjen Arandjelović, and Jakob Nikolas Kather. Benchmarking pathology feature extractors for whole slide image classification. *arXiv preprint arXiv:2311.11772v5*, 2024. 1
- [46] Hanwen Xu, Naoto Usuyama, Jaspreet Bagga, Sheng Zhang, Rajesh Rao, Tristan Naumann, Cliff Wong, Zelalem Gero, Javier González, Yu Gu, et al. A whole-slide foundation model for digital pathology from real-world data. *Nature*, pages 1–8, 2024. 1, 5
- [47] Jiahui Yu, Zirui Wang, Vijay Vasudevan, Legg Yeung, Mojtaba Seyedhosseini, and Yonghui Wu. Coca: Contrastive captioners are image-text foundation models. *Transactions on Machine Learning Research (TMLR)*, 2022. 7
- [48] Jinghao Zhou, Chen Wei, Huiyu Wang, Wei Shen, Cihang Xie, Alan Yuille, and Tao Kong. Image BERT pre-training with online tokenizer. In *International Conference on Learning Representations (ICLR)*, 2022. 7
- [49] Eric Zimmermann, Eugene Vorontsov, Julian Viret, Adam Casson, Michal Zelechowski, George Shaikovski, Neil Tenenholtz, James Hall, Thomas Fuchs, Nicolo Fusi, et al. Virchow2: Scaling self-supervised mixed magnification models in pathology. *arXiv preprint arXiv:2408.00738*, 2024. 1, 5

Evaluating Computational Pathology Foundation Models for Prostate Cancer Grading under Distribution Shifts

Supplementary Material

A. Supplementary Tables

Table S1. Raw numerical results for Figure 1. All results are mean±std over 10 random cross-validation folds.

	PANDA	Karolinska	Radboud	Radboud → Karolinska	Radboud-U	Radboud-U → Karolinska-U	Radboud-L	Radboud-L → Radboud-R
UNI - <i>ABMIL</i>	0.888±0.013	0.886±0.009	0.853±0.026	0.247±0.138	0.843±0.023	0.459±0.112	0.826±0.036	0.739±0.014
CONCH - <i>ABMIL</i>	0.866±0.009	0.862±0.015	0.818±0.021	0.024±0.018	0.818±0.028	0.206±0.075	0.805±0.048	0.712±0.014
Resnet-IN - <i>ABMIL</i>	0.773±0.013	0.750±0.027	0.726±0.023	0.185±0.041	0.725±0.018	0.380±0.035	0.708±0.046	0.545±0.014
UNI - <i>Mean Feature</i>	0.845±0.020	0.779±0.021	0.846±0.015	0.489±0.059	0.828±0.028	0.516±0.018	0.806±0.032	0.686±0.020
CONCH - <i>Mean Feature</i>	0.777±0.019	0.714±0.023	0.743±0.025	0.026±0.015	0.743±0.038	0.165±0.048	0.731±0.055	0.590±0.019
Resnet-IN - <i>Mean Feature</i>	0.610±0.030	0.484±0.041	0.565±0.023	0.216±0.023	0.550±0.040	0.369±0.006	0.514±0.045	0.425±0.006
UNI - <i>kNN</i>	0.727±0.018	0.582±0.033	0.747±0.027	0.214±0.037	0.711±0.036	0.283±0.034	0.666±0.030	0.397±0.005
CONCH - <i>kNN</i>	0.690±0.021	0.590±0.026	0.687±0.041	0.208±0.012	0.665±0.030	0.320±0.023	0.630±0.043	0.387±0.008
Resnet-IN - <i>kNN</i>	0.613±0.016	0.461±0.030	0.630±0.042	0.070±0.013	0.594±0.048	0.098±0.029	0.502±0.041	0.282±0.008

Table S2. Raw numerical results for Figure 2. All results are mean±std over 10 random cross-validation folds.

	PANDA	Karolinska	Radboud	Radboud → Karolinska	Radboud-U	Radboud-U → Karolinska-U	Radboud-L	Radboud-L → Radboud-R
<i>ABMIL</i> - UNI	0.888±0.013	0.886±0.009	0.853±0.026	0.247±0.138	0.843±0.023	0.459±0.112	0.826±0.036	0.739±0.014
<i>Mean Feature</i> - UNI	0.845±0.020	0.779±0.021	0.846±0.015	0.489±0.059	0.828±0.028	0.516±0.018	0.806±0.032	0.686±0.020
<i>kNN</i> - UNI	0.727±0.018	0.582±0.033	0.747±0.027	0.214±0.037	0.711±0.036	0.283±0.034	0.666±0.030	0.397±0.005
<i>ABMIL</i> - CONCH	0.866±0.009	0.862±0.015	0.818±0.021	0.024±0.018	0.818±0.028	0.206±0.075	0.805±0.048	0.712±0.014
<i>Mean Feature</i> - CONCH	0.777±0.019	0.714±0.023	0.743±0.025	0.026±0.015	0.743±0.038	0.165±0.048	0.731±0.055	0.590±0.019
<i>kNN</i> - CONCH	0.690±0.021	0.590±0.026	0.687±0.041	0.208±0.012	0.665±0.030	0.320±0.023	0.630±0.043	0.387±0.008
<i>ABMIL</i> - Resnet-IN	0.773±0.013	0.750±0.027	0.726±0.023	0.185±0.041	0.725±0.018	0.380±0.035	0.708±0.046	0.545±0.014
<i>Mean Feature</i> - Resnet-IN	0.610±0.030	0.484±0.041	0.565±0.023	0.216±0.023	0.550±0.040	0.369±0.006	0.514±0.045	0.425±0.006
<i>kNN</i> - Resnet-IN	0.613±0.016	0.461±0.030	0.630±0.042	0.070±0.013	0.594±0.048	0.098±0.029	0.502±0.041	0.282±0.008

B. Supplementary Figures

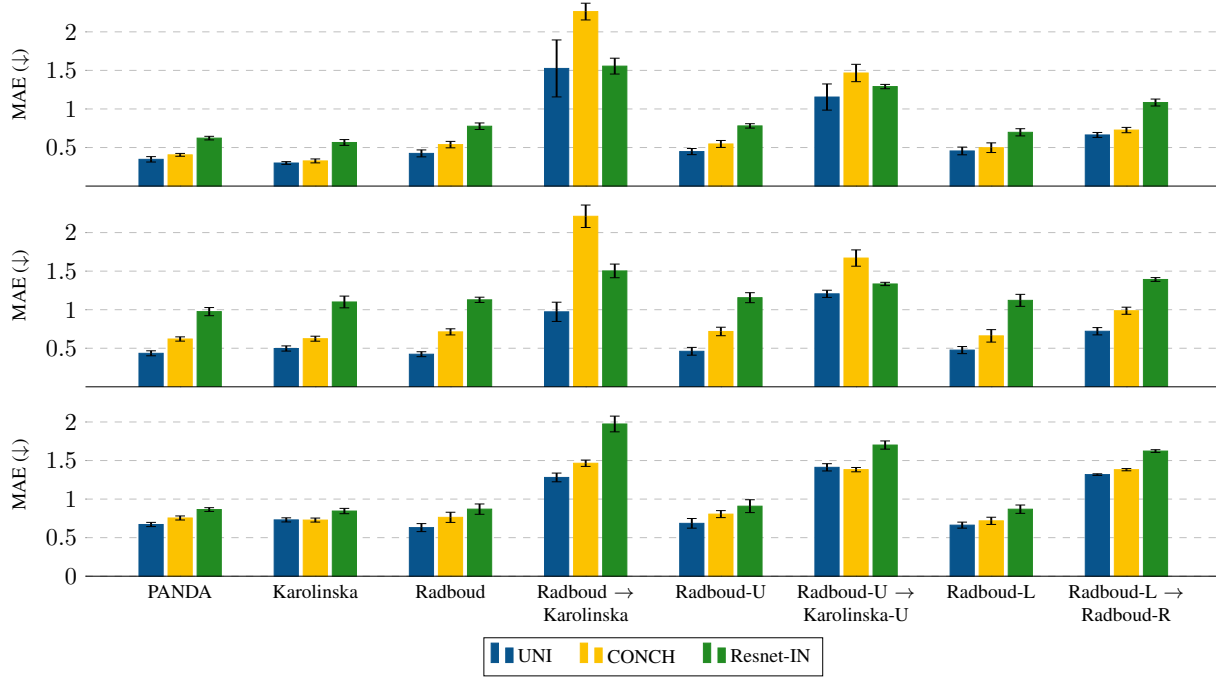


Figure S1. Performance comparison of UNI, CONCH and Resnet-IN across different PANDA subset, when utilized as patch-level feature extractors in the *ABMIL* (top), *Mean Feature* (middle) or *kNN* (bottom) ISUP grade models. The same comparison as in Figure 1, but in terms of MAE (lower is better) instead of kappa. The ranking of UNI, CONCH and Resnet-IN is virtually identical as in Figure 1.

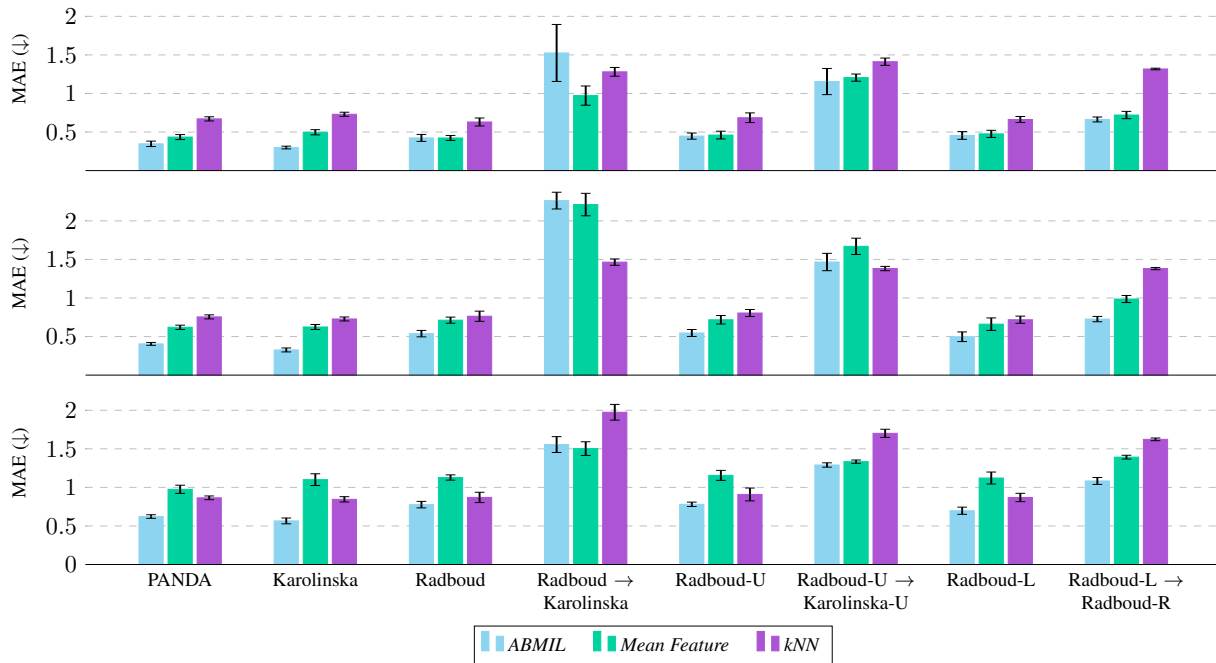


Figure S2. Performance comparison of the ISUP grade models *ABMIL*, *Mean Feature* and *kNN*, when utilizing UNI (top), CONCH (middle) or Resnet-IN (bottom) as patch-level feature extractors. The same comparison as in Figure 2, but in terms of MAE (lower is better) instead of kappa. The ranking of *ABMIL*, *Mean Feature* and *kNN* is virtually identical as in Figure 2.